communications biology

A Nature Portfolio journal

Article

https://doi.org/10.1038/s42003-026-10282-0

Genetic risk of Alzheimer's disease is associated with loss of brain network segregation in midlife

Feng Deng[1], Richard N. Henson[2,3], Graciela Muniz-Terrera[4,5], Paresh Malhotra[6,7], John T. O'Brien[3,8], Craig W. Ritchie[4,9], Brian Lawlor[10,11] & Lorina Naci[10,11]

Alzheimer's disease (AD) neuropathology starts decades before clinical manifestations, but the early indicators of AD in midlife remain unclear. Functional segregation of brain networks is a key marker of brain health. It remains unknown, however, whether inherited risk of AD impacts network segregation from midlife in individuals who are cognitively healthy but carry inherited risk for late-life AD. To address this question, we investigate which brain networks show the strongest age-related segregation loss in the Cam-CAN lifespan cohort (18–88 years, $N = 652$), and whether *APOE* ε4 genotype impacts segregation of age-vulnerable networks in the midlife PREVENT cohort (40–59 years, $N = 210$), cross-sectionally and longitudinally. Higher-order networks showing the most significant age-related decline are the default mode (DMN), frontal-parietal control (FPN) and salience (SN) networks. Cognitively healthy midlife *APOE* ε4 carriers have higher segregation across the brain cross-sectionally, accompanied by greater longitudinal decline in the DMN over two years, relative to non-carriers. Higher DMN segregation is associated with better episodic and relational memory across the PREVENT cohort. These findings suggest that functional segregation may serve as a potential biomarker, providing insights into the mechanisms through which *APOE* influences brain function and cognition from healthy midlife, on average 23 years before dementia onset.

Dementia, particularly Alzheimer's disease (AD), is a growing public health concern that presents profound challenges to healthcare systems, families and societies throughout the world[1]. Midlife is a critical period for the development of AD pathology[2,3] and potentially, a disease-altering window prior to the manifestation of substantial brain damage. There is an urgent need for risk reduction interventions focused on midlife[4–6]. However, the indicators and brain mechanisms of AD in midlife remain poorly understood[7,8].

Accumulating evidence points to functional brain network segregation —the extent to which a network is distinct from others in its functional connectivity profile—as a marker of brain health in both normal and pathological ageing. Increasing adult age is associated with reduced network segregation[9–13], and such 'dedifferentiation' is in turn associated with age-related decline in cognitive and motor function[10,12,14–19]. Conversely, preservation of network segregation is associated with maintenance of cognition in healthy ageing[20–22] and in patients with brain injury[23], suggesting that functional network segregation supports cognitive reserve[24]. In asymptomatic older adults (mean age >65 years), loss of network segregation was associated with the accumulation of AD pathology, such as beta-amyloid (Aβ) and tau[25,26], or the presence of apolipoprotein (*APOE*) ε4 allele[27], the main genetic risk factor for sporadic late-onset AD in the Indo-European population[28]. Reduction of network segregation in *APOE* ε4 carriers was also associated with cognitive decline[27], and, conversely, its maintenance was associated with preserved cognitive performance, despite the presence of AD pathology[26]. Decreased segregation was also observed in patients with mild cognitive decline (MCI)[29,30] and AD[26,31] compared to age-matched controls. An accelerated decline in network segregation with ageing has been associated with increasing dementia severity[21].

[1]School of Psychology, Shenzhen University, Shenzhen, China. [2]Medical Research Council Cognition and Brain Sciences Unit, University of Cambridge, Cambridge, UK. [3]Department of Psychiatry, School of Clinical Medicine, University of Cambridge, Cambridge, UK. [4]Edinburgh Dementia Prevention, University of Edinburgh, Edinburgh, UK. [5]Department of Social Medicine, Ohio University, Ohio, Athens, OH, USA. [6]Department of Brain Science, Imperial College London, London, UK. [7]UK Dementia Research Institute Care Research and Technology Centre, Imperial College London and the University of Surrey, London, UK. [8]Cambridgeshire and Peterborough NHS Foundation Trust, Cambridge, UK. [9]Scottish Brain Sciences, Edinburgh, UK. [10]Trinity College Institute of Neuroscience, School of Psychology, Trinity College Dublin, Dublin, Ireland. [11]Global Brain Health Institute, Trinity College Dublin, Dublin, Ireland. e-mail: nacil@tcd.ie

Table 1 | Demographic information for the Cam-CAN cohort

		Whole cohort
Age range, y		18–88
Sex (Female), %		50.61
Education[a]	University	395
	A Levels	68
	GCSE	111
	None	75

[a]Education levels were categorized according to the British education system: '*none*' no education over the age of 16 years; '*GCSE*' General Certificate of Secondary Education; '*A Levels*' General Certificate of Education Advanced Level; '*University*' undergraduate or graduate degree (where higher levels subsume lower ones). Educational information was missing for 3 participants.

It remains unknown, however, whether network segregation shows early modifications, from midlife, in individuals who have inherited risk of Alzheimer's disease but are presently cognitively healthy. This question has important implications for identifying intermediate phenotypes of the earliest brain changes in the preclinical stages of AD[32], which can provide urgently needed early disease biomarkers for timely preventative interventions from midlife. It is also not known which brain networks are more liable to segregation loss during healthy ageing and in preclinical AD populations. Associative networks are shown to be more susceptible to age-related 'dedifferentiation' than the sensorimotor networks[10,11,17,33–35], but it is not known which individual network show early risk-related changes from midlife. The default mode network (DMN) is one such candidate network[36–39], with early changes—atrophy and metabolic abnormalities—being found in its core regions at early stages of clinical AD progression[40–42].

To address these gaps, this study first investigated the age-related effects on individual network segregation among a comprehensive set of ten atlas-based[43] brain networks. We leveraged the large functional Magnetic Resonance Imaging (fMRI) dataset of healthy individuals ($N = 652$ aged 18–88) from the Cambridge Centre for Ageing and Neuroscience (Cam-CAN, www.cam-can.org). Second, we examined in a subset of brain networks identified from the Cam-CAN analyses, the cross-sectional and longitudinal effects of inherited risk for late-life AD in cognitively healthy midlife individuals ($N = 210$ aged 40–59 years) from the PREVENT Dementia programme (https://preventdementia.co.uk/). The behavioural significance of network segregation in each cohort was tested via the relationship between network segregation and cognition, using comparable cognitive measures, i.e., fluid intelligence and episodic memory in Cam-CAN and episodic and relational memory in PREVENT.

We predicted age-related loss of segregation globally, and in specific associative networks, particularly in the DMN, and that network segregation would be significantly associated with cognitive performance. *APOE* ε4 carriers were predicted to show reduced network-specific segregation relative to *APOE* ε4 non-carriers cross-sectionally, and loss of segregation longitudinally, over the 2-year period, in the DMN.

Results

Demographic characteristics for the Cam-CAN cohort

Demographic characteristics of the Cam-CAN cohort are shown in Table 1.

Functional network segregation across the healthy adult lifespan in the Cam-CAN cohort

Global segregation in the Cam-CAN cohort. Global segregation showed a significant linear effect of age. The mean participation coefficient (Pc) across all region of interests (ROIs) increased with age ($\beta = 0.28$, $p < 0.001$, Fig. 1 and Table 2), adjusted for sex and mean frame-wise displacement (FD). Any quadratic effect of age did not reach significance. This result was also supported by the validation analyses using the Raichle atlas [see Supplementary Information (SI)]. Females had a small effect of significantly lower Pc values ($\beta = -0.08$, $p < 0.05$), or stronger network segregation than males. The linear Pc-Age relationship

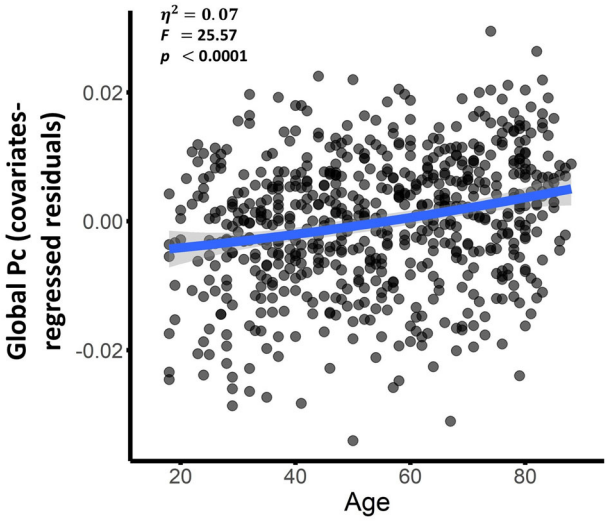

Fig. 1 | Associations between global participation coefficient (Pc) and age in the Cam-CAN cohort ($N = 652$). Global Pc values (y-axis) were adjusted for sex and head movement. Higher Pc reflects decreased network segregation.

remained significant ($\beta = 0.19$, $p = 0.004$) when additionally controlling for total intracranial volume (TIV, i.e., head size), and for grey matter volume (GMV, see Supplementary Table 1), a standard measure of brain health, suggesting that the Pc measure captures additional effects of age of functional network organization.

Network-level segregation in the Cam-CAN cohort. To investigate whether segregation of individual networks was selectively vulnerable to healthy ageing, we assessed the effects of age on the mean Pc within each of the ten networks separately, adjusted for sex and mean FD. A second-order polynomial expansion of age showed a significant linear effect of age on 5/10 networks (Fig. 2), with frontal-parietal control (FPN, $\beta = 0.34$, $p < 0.001$), default mode (DMN, $\beta = 0.25$, $p < 0.001$), salience (SN, $\beta = 0.25$, $p < 0.001$), and visual (VIS, $\beta = 0.20$, $p < 0.001$) networks showing an increase in Pc (reduced segregation) with age, and SM1 (sensorimotor hand, $\beta = -0.20$, $p < 0.001$) showing a decrease in Pc (increased segregation) with age. There was also a significant quadratic age effect on Pc of FPN ($\beta = 0.14$, $p < 0.001$, Fig. 2). The other networks showed no significant associations with age after Bonferroni-correction for the number of networks. The result that the three higher-order networks (FPN, DMN, SN) were particularly susceptible to age-related changes was also corroborated by the validation analyses using the Raichle atlas (Supplementary Fig. 1).

The results for the three higher-order networks (FPN, DMN, SN) were consistent with our expectations, based on prior literature on age-related segregation loss on associative networks[10]. The effect of age on the functional segregation of the Motor 1 network was not related to the study question, thus was not examined further, though may be of interest for future studies. A supporting analysis confirmed that the same three networks show the strongest effect of age in the PREVENT cohort (Supplementary Fig. 2).

Network segregation and cognitive performance in the Cam-CAN cohort

Global Pc and the Pc of FPN, DMN and SN were significantly related to fluid intelligence and episodic memory, after controlling for sex and mean FD, indicating that lower segregation was significantly associated with poorer cognitive performance. When additionally accounting for the linear and quadratic effects of age, the associations between Pc and cognition were no longer significant. Therefore, we cannot be confident whether the initial associations reflect true effects or merely driven by age-related confounding (see SI for full results).

Table 2 | Regression models assessing associations of global participation coefficient (Pc) with age, controlling for covariates, in the Cam-CAN cohort

Dependent variables	Independent variables	*β*	95% CI	*t*	*p*
Global Pc	Age	0.28	[0.20, 0.36]	7.13	<0.001
	Age^2	0.02	[−0.05, 0.09]	0.52	0.60
	Sex	−0.08	[−0.15, −0.01]	−2.32	0.02
	Mean FD	0.25	[0.17, 0.32]	6.28	<0.001

β standardised coefficient, *CI* confidence interval, *FD* framewise displacement.

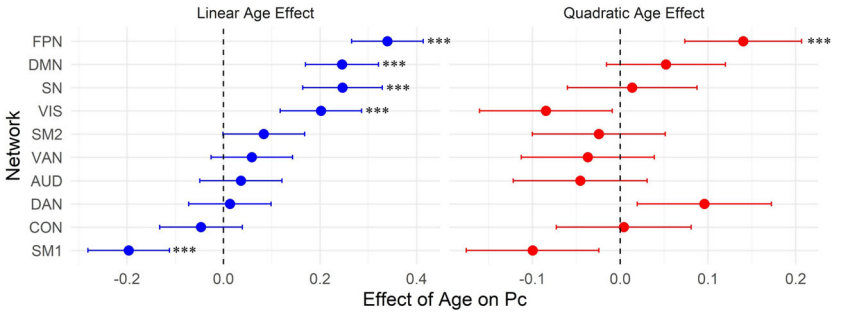

Fig. 2 | Network-specific effect of age on participation coefficient (Pc), adjusted for sex and head motion in the Cam-CAN cohort ($N = 652$). Standardized β coefficient (dot) and 95% confidence interval (CI, horizontal line) are shown for each network. Positive β coefficient reflects an inverse relationship between network segregation and age, as higher Pc values indicate reduced network segregation. *** indicates $p < 0.005$ (Bonferonni-corrected for the 10 networks). FPN frontal-parietal control, DMN default mode, SN salience, VIS visual, SM somatomotor, VAN ventral attention, AUD auditory, DAN dorsal attention, CON cingulo-opercular control.

Table 3 | Demographic information for the PREVENT cohort in baseline and follow-up (over 2 years) samples, stratified by *APOE* genotype

		APOE ε4+	*APOE* ε4−	*p* value
Baseline ($N = 153$)	Sample size	54	99	–
	Age, y	52.00 (7.00)	53.00 (9.50)	0.31
	Sex (Female), %	70.37%	71.72%	1.00
	Years of education	17.00 (4.75)	16.00 (5.00)	0.21
Follow-up ($N = 149$)	Sample size	57	92	–
	Age, y	54.00 (7.00)	55.00 (8.00)	0.17
	Sex (Female), %	77.19%	71.74%	0.59
	Years of education	17.00 (4.00)	16.00 (4.25)	0.55

Values shown are the median (interquartile range, IQR) where applicable. *p* values were obtained from Mann–Whitney tests for continuous variables and from chi-squared tests for categorical variables.
APOE ε4+ Apolipoprotein ε4 genotype positive, *APOE ε4−* Apolipoprotein ε4 genotype negative.

Demographic characteristics for the PREVENT cohort

The demographic information for the PREVENT cohort that passed quality control, at baseline and at follow-up is shown in Table 3. Participants are stratified by *APOE*ε4 genotype. There were no significant differences in age, sex or years of education (Table 3).

Network segregation and the *APOE* risk factor in the PREVENT cohort at baseline

Global segregation in the PREVENT cohort at baseline. The multiple regression model for the *APOE* risk factor showed a significant negative association between global Pc and *APOE* ε4 genotype ($\beta = -0.18$, $p = 0.03$), after adjusting for effects of age, sex, mean FD and number of brain nodes (owing to differences in the field of view, see 'Methods') (Table 4). The effect of *APOE* remained significant when adding GMV and TIV as covariates ($\beta = -0.18$, $p = 0.03$), suggesting the effect of *APOE* on segregation is independent of any effect of *APOE* on grey matter volume. *APOE* ε4 carriers had significantly higher segregation than ε4 non-carriers (Fig. 3a). Furthermore, the *APOE* effect remained robust after controlling for both linear and quadratic age effects, as well as the aforementioned covariates (see SI). The inclusion of an additional second-order polynomial expansion of age covariate was to account for the nonlinear age-related changes in Pc observed in our broader analyses (see SI). This result was further supported by validation analyses using a second brain parcellation scheme by Raichle (2011) (Supplementary Table 2) and the mutual information connectivity metric (see SI). Moreover, this result was not merely attributable to overall connectivity differences (see SI).

Network-level segregation in the PREVENT cohort at baseline. To test whether the effect of *APOE* ε4 genotype was specific to certain high-level network(s), we investigated each of the three associative networks identified as showing age and cognition effects in the independent Cam-CAN dataset. Only the DMN showed a significant negative association between *APOE* ε4 genotype and Pc at baseline ($\beta = -0.19$, $p = 0.01$), independent of age, sex, mean FD and number of brain nodes (Fig. 3b), with Bonferroni correction. This result remained robust after controlling for both linear and quadratic age effects, as well as the aforementioned covariates (see SI). This result was also supported by the validation analyses using the Raichle atlas (Supplementary Table 2) and the mutual information connectivity metric (see SI). Moreover, this result was not merely attributable to overall connectivity differences (see SI). Additionally, DMN segregation was highly consistent across the Power and Raichle atlases (Supplementary Fig. 3), which suggests that this measure is robust.

The other two networks did not show significant associations with *APOE* genotype (FPN: $\beta = -0.11$, $p = 0.21$; SN: $\beta = -0.09$, $p = 0.28$). We also found no significant differences in either global efficiency or modularity between *APOE* ε4 carriers and non-carriers, suggesting that global network topology remains largely intact at this midlife stage (see SI).

Network segregation and cognitive performance in the PREVENT cohort at baseline

We then examined the associations between global and DMN segregation and cognitive performance. At baseline, there was a significant negative,

Table 4 | Associations between age and the main genetic risk factor *APOE* ε4 allele with global participation coefficient (Pc) in the PREVENT cohort at baseline

Dependent variables	Independent variables	β	95% CI	t	p
Global Pc	*APOE* ε4	−0.18	[−0.34, −0.02]	−2.26	0.03
	Age	0.02	[−0.13, 0.17]	0.28	0.78
	Sex	−0.14	[−0.31, 0.02]	−1.74	0.08
	Mean FD	0.28	[0.12, 0.43]	3.61	0.0004
	No. of brain nodes	0.17	[0.02, 0.32]	2.21	0.03

Standard coefficient β was reported.
CI confidence interval, *FD* framewise displacement.

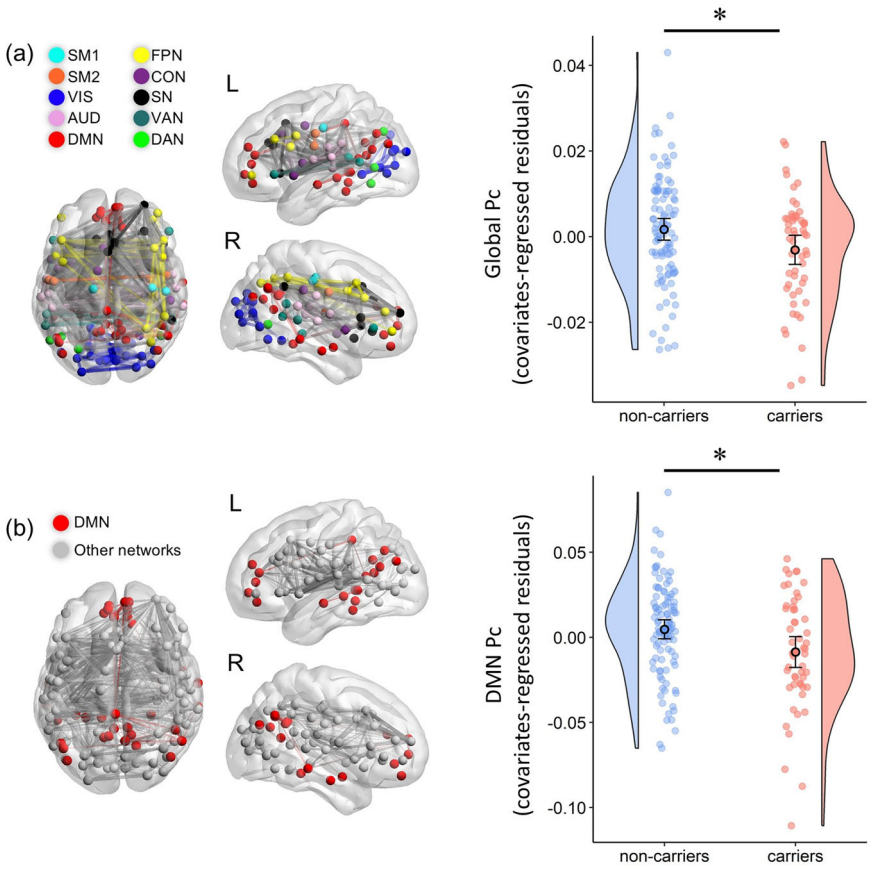

Fig. 3 | Cross-sectional associations between *APOE* ε4 allele and participation coefficient (Pc) of functional brain networks in the PREVENT cohort ($N = 54$ carriers and $N = 99$ non-carriers). Brain nodes of 10 predefined networks retained for a sample participant were displayed in a 3D glass brain (left panel) for visualization purposes only. Coloured lines represent the functional connectivity within particular networks (e.g., red for DMN) and grey lines represent the between network functional connectivity. **a** *APOE* ε4 carriers had lower global Pc (higher segregation) relative to non-carriers. Global Pc was residuals adjusted for age, sex, head motion and number of brain nodes. **b** *APOE* ε4 carriers had lower Pc (higher segregation) of the default mode network (DMN) relative to non-carriers. The error bars represent the mean ± standard error of the mean for each group. FPN frontal-parietal control, DMN default mode, SN salience, VIS visual, SM somatomotor, VAN ventral attention, AUD auditory, DAN dorsal attention, CON cingulo-opercular control. *$p < 0.05$, FWE corrected.

cross-sectional association between global Pc and episodic/relational memory ($\beta = -0.16$, $p = 0.04$), independent of the effects of age, sex, years of education, mean FD and number of brain nodes. Lower functional segregation (higher Pc) was associated with worse memory (Fig. 4a). The effect was observed for the segregation of the DMN, with a significant negative relationship with episodic/relational memory ($\beta = -0.19$, $p = 0.03$, Fig. 4b). There were no significant differences in these relationships between *APOE* ε4 carriers and non-carriers (see SI).

Longitudinal effects of the *APOE* genotype on network segregation in the PREVENT cohort

We asked whether longitudinal changes in global and DMN segregation were associated with *APOE* ε4 allele carriership. Time × *APOE* ε4 interaction for global Pc did not reach significance (Table 5, Fig. 5a). We found a significant interaction of time × *APOE* ε4 for DMN Pc ($\beta = 0.10$, $p = 0.03$, Table 5). Paired *t*-tests showed that only *APOE* ε4 carriers had a significant increase in DMN Pc (loss of network segregation) over 2 years ($t = -2.38$, $p = 0.02$), with *APOE* ε4 non-carriers showing no significant longitudinal change (Fig. 5b). Note that global Pc showed a similar trend, even if not significant (Fig. 5a). Longitudinally, there was no significant association between changes in episodic/relational memory over the 2 years and changes in either global Pc or DMN Pc.

Discussion

Functional segregation of brain networks has recently emerged as a key marker of brain health. It remains unknown whether network segregation shows early modifications in midlife individuals with inherited risk of late-life Alzheimer's disease, and thus whether it can serve as a biomarker of preclinical AD in at-risk individuals. To address this question, in the first instance, we investigated which brain networks show the strongest age-related loss of segregation, in the large-scale Cam-CAN lifespan cohort (18–88 years, $N = 652$). The three higher-order networks that showed the most significant age-related decline were the FPN, SN and DMN. Subsequently, we investigated in these three age-vulnerable associative networks, whether *APOE* ε4 genotype impacts network segregation in the cognitively healthy PREVENT cohort (40–59 years, $N = 210$). The DMN was of

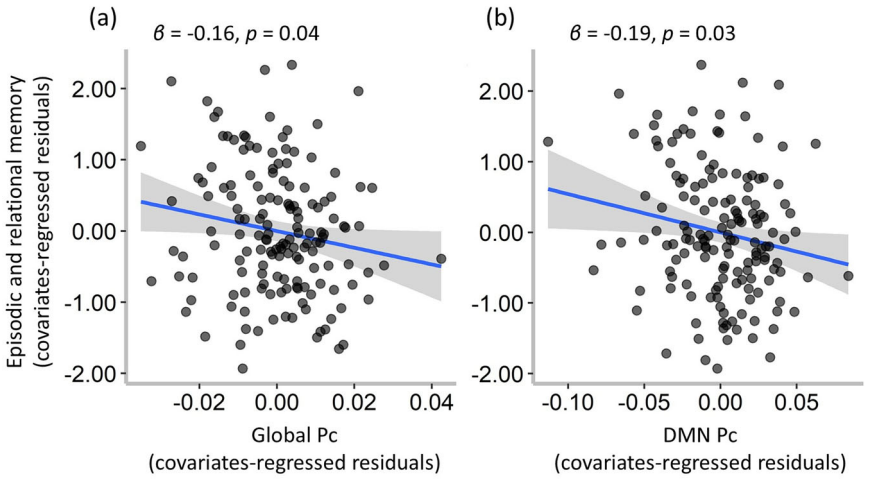

Fig. 4 | Cross-sectional relationships between participation coefficient (Pc) and cognitive performance in the PREVENT cohort ($N = 155$, including two participants for whom *APOE* genotyping information was unavailable). a Global Pc and **b** DMN Pc on the y-axis were adjusted for age, sex, years of education, head motion and number of brain nodes. Higher Pc values indicate reduced network segregation.

Table 5 | Longitudinal changes (over 2 years) in global and default model network (DMN) participation coefficient in relation to apolipoprotein ε4 (*APOE* ε4) allele in the PREVENT cohort

Dependent variables	Independent variables	*β*	95% CI	*t*	*p*
Global Pc	Time	0.09	[−0.01, 0.19]	1.68	0.09
	APOE ε4	−0.19	[−0.33, −0.05]	−2.57	0.01
	Time × *APOE*ε4	0.04	[−0.06, 0.14]	0.84	0.40
	Age at baseline	0.07	[−0.06, 0.21]	1.02	0.31
	Sex	−0.08	[−0.23, 0.08]	−0.99	0.33
	Mean FD	0.27	[0.14, 0.40]	3.99	<0.001
	No. of brain nodes	0.20	[0.08, 0.33]	3.26	0.001
DMN Pc	Time	0.01	[−0.08, 0.10]	0.22	0.82
	APOE ε4	−0.16	[−0.29, −0.02]	−2.17	0.03
	Time × *APOE*ε4	0.10	[0.01, 0.19]	2.16	0.03
	Age at baseline	−0.001	[−0.14, 0.13]	−0.02	0.99
	Sex	−0.10	[−0.25, 0.06]	−1.23	0.22
	Mean FD	0.35	[0.23, 0.48]	5.40	<0.001
	No. of brain nodes	−0.16	[−0.28, −0.04]	−2.69	0.01

Standard coefficient β was reported.
*CI*confidence interval, *FD* framewise displacement.

particular interest for follow-up in individuals with inherited risk for late-life AD, given previous findings of DMN changes in early clinical Alzheimer's pathology[36,37,44–46].

The main novel finding of this study was that cognitively healthy *APOE* ε4 carriers had higher segregation cross-sectionally across the brain, accompanied by decline of segregation longitudinally over two years, relative to non-carriers, in the DMN. Higher segregation of the DMN was also associated with better episodic and relational memory cross-sectionally across the PREVENT cohort. These results were supported by validation analyses using an independent brain atlas. Although the direction of the cross-sectional effect was contrary to our prediction, it aligns with other findings for *APOE* ε4 carriers in midlife cohorts, including stronger cognition[8,47–49], cerebral hyperperfusion[50–52], and hyperconnectivity within the DMN[53,54], relative to non-carriers. Furthermore, Koelewijn et al.[55] found significantly higher functional connectivity of brain networks as measured with MEG, particularly in the DMN, in young *APOE* ε4 carriers (age: 24.5 ± 5.4 years) compared to age-matched non-carriers[55], but significantly reduced functional connectivity in clinical AD patients (age: 67–89 years) compared to age-matched healthy controls[56]. These results are consistent with the antagonistic pleiotropy hypothesis of aging[57], which proposes that deleterious genes, such as the *APOE* ε4 gene allele, have survived through evolution because they might confer an advantage early in life, when humans are reproductively fit.

To the best of our knowledge, this is the first study to show a prominent decline in functional segregation of the DMN longitudinally in cognitively healthy individuals at risk for late-onset AD in midlife. This advances previous literature, showing a greater age-related segregation loss in older adults *APOE* ε4 carriers (58–79 years) compared to non-carriers[27], and, that in older adults (> 65 years), age-related loss of network segregation predicted dementia severity[21]. Several inter-related brain mechanisms may underlie this age- and genetic risk-related de-segregation, including degradation of white matter integrity[58], vascular disease leading to weaker long-range connectivity[58], and dopaminergic decline[59]. Our findings significantly advance this literature, by demonstrating that inherited risk of late life AD is associated with longitudinal loss of segregation in the DMN, in cognitively healthy individuals, on average 23 years before the onset of dementia symptoms, based on the parental age at the onset of dementia symptoms in this cohort. In summary, the convergence on the DMN as the second most vulnerable network to age-related segregation loss (in Cam-CAN) and the brain network to show a longitudinal effect of *APOE* ε4 genotype (in PREVENT), provides strong evidence that, from midlife, the functional

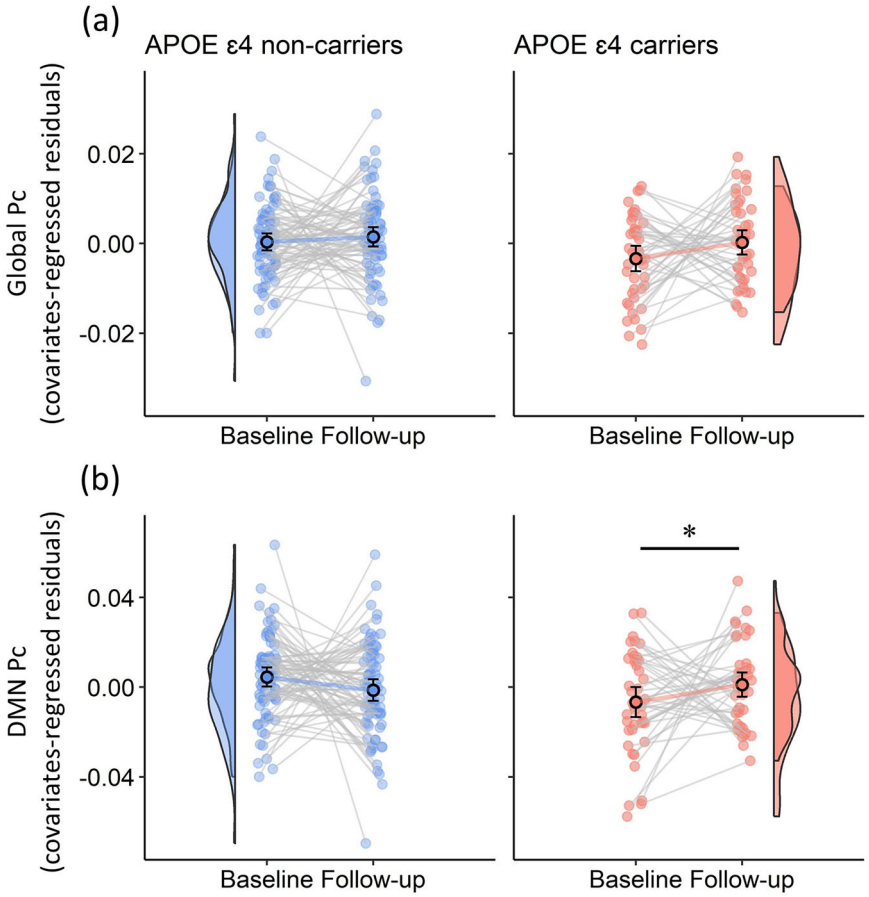

Fig. 5 | Longitudinal associations between *APOE* ε4 allele and participation coefficient (Pc) of functional brain networks over 2 years in the PREVENT cohort ($N = 45$ carriers and $N = 78$ non-carriers). **a** No significant change in global Pc for either group. **b** *APOE* ε4 carriers only showed significantly increased Pc (decreased segregation) of the default mode network (DMN). Pc was adjusted for effects of age, sex, head motion and number of brain nodes. $^*p < 0.05$. The error bars represent the mean ± standard error of the mean for each group.

architecture of the DMN is vulnerable to aging and genetic risk of late-life AD.

In contrast to the longitudinal decline in functional segregation of the DMN, episodic memory did not show significant decline over the 2-year follow-up period in this cognitively healthy midlife cohort. This dissociation suggests that alterations in functional network segregation may precede detectable cognitive decline, supporting the view that segregation loss represents an early neural vulnerability marker rather than a contemporaneous correlate of cognitive change. It is also possible that the relatively short interval (2 years) between assessments limited our ability to capture subtle or emerging cognitive changes at this preclinical stage, when cognitive performance is largely preserved.

We further found that this earliest genetic risk signature on the midlife brain is not a system-wide topological decline, as reflected by preserved global efficiency and modularity, but a more localized alteration in the connectivity profile of DMN nodes. This nuanced change in the DMN may reflect a period of functional compensation that precedes the system-level dedifferentiation observed in later stages of Alzheimer's disease[26].

We additionally observed a trend-level sex effect on global participation coefficient in the PREVENT cohort (Table 4), with females exhibiting higher functional segregation relative to males at baseline. Although this effect did not reach statistical significance in the present sample, it suggests a potential sex-related difference in large-scale network organization during midlife. Given the established sex differences in Alzheimer's disease risk and trajectory, this finding warrants further longitudinal investigation in the larger PREVENT cohort ($N = 700$) which is currently in the visit 3 testing phase. Future studies from this cohort will be key for establishing whether sex moderates the relationship between functional segregation, genetic risk, and longitudinal cognitive outcomes.

Greater network segregation in the DMN was significantly associated with better episodic and relational memory. The DMN has been recognized for its critical role in episodic memory[60], and our findings further suggest that maintaining functional segregation of the DMN may be crucial for protecting episodic memory from midlife. Taken together, these results suggest an impact of the genetic risk for late-life sporadic AD on loss of functional segregation across the brain and in the DMN, as well as a role for segregation loss in the DMN as a mechanism for incipient impairment of episodic memory, from midlife. Thus, they highlight the importance of studying the origins of Alzheimer's disease in this age group, an estimated 23 years from typical symptoms onset.

Methodological considerations

We did not find a significant association between longitudinal change in network segregation and change in cognition over two years, which may be due to the relatively short follow-up period. Future studies from the ongoing third testing waves (8 years post baseline, respectively) of the PREVENT cohort will determine the longitudinal impact of inherited AD risk on the cognitive trajectories and their relationship to changes in network segregation. The results of the present study were controlled for a small significant effect of sex on global network segregation, with females showing higher network segregation than males in the Cam-CAN cohort, independent of a second-order polynomial expansion of age. Presently, there is a dearth of knowledge on sex differences in network segregation. This finding highlights the importance of taking into consideration in future studies sex differences in network segregation, which may help to explain sex differences in the prevalence and progression of Alzheimer's disease. The study population are mainly (95%) of white Caucasian ethnicity, not dissimilar to the historic ethnic mix of older people in the UK and Ireland, which limits generalizability of findings beyond individuals of European ancestry.

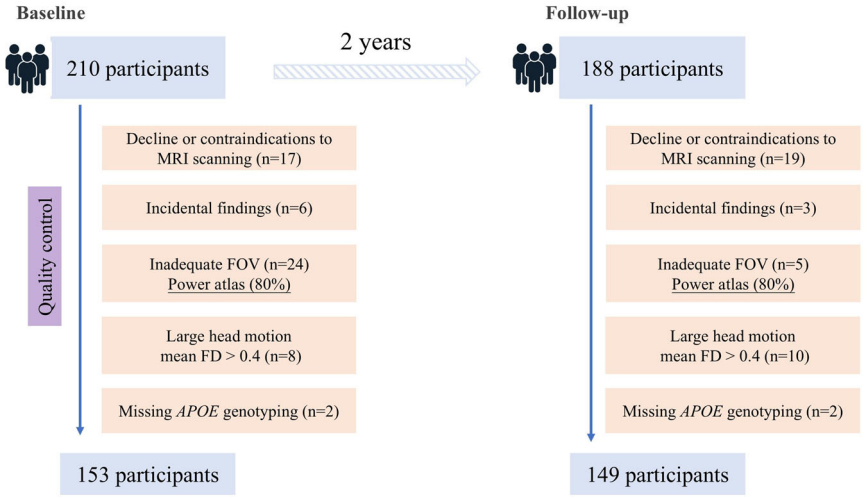

Fig. 6 | Participant exclusions for fMRI data analyses of the PREVENT cohort. FOV field of view, FD framewise displacement.

Conclusion

In conclusion, this study provides evidence for selective vulnerability of specific associative brain networks in healthy ageing and in midlife individuals with inherited risk for late-onset AD. Results suggest an early impact of the genetic risk for late-life sporadic AD on loss of functional segregation across the brain, and in the DMN, as well as role for segregation loss in the DMN as a mechanism for incipient impairment of episodic memory, from midlife. Thus, they suggest that functional segregation serves as a potential biomarker, and provides valuable insights into the underlying mechanisms through which *APOE* influences brain function and cognition from healthy midlife years. Furthermore, these suggest that functional network architecture changes can serve as an earlier and complementary indicator of vulnerability to late-life AD risk, relative to cerebral spinal fluid (CSF)[61,62] and blood-based biomarkers[63,64]—potentially identifying at-risk individuals long before conventional pathological changes can be measured in the prodromal disease stages.

Methods

Participants

Healthy adult lifespan in Cam-CAN. The healthy lifespan cohort was drawn from the Cam-CAN research programme (http://www.cam-can.org/), a large-scale collaborative research project aimed at elucidating the neurocognitive mechanisms that underpin healthy cognitive ageing. A detailed protocol has been described elsewhere[65]. Ethical approval was obtained from the Cambridgeshire 2 (now East of England-Cambridge Central) Research Ethics Committee, and informed consent was obtained from all participants prior to assessments and imaging. All ethical regulations relevant to human research participants were followed. The cohort consisted of healthy volunteers aged 18–88 years. Data collected in the second phase of this project were examined in the present study. 652 participants (322 male; 330 female) underwent structural and resting-state fMRI scans.

Middle-aged adults at risk of AD in PREVENT Dementia research programme. The PREVENT Dementia programme is an ongoing longitudinal study investigating the origins and early diagnosis of dementia in midlife at-risk individuals[66]. The data used in this study represent the first phase of the programme ($N = 210$), collected at the West London National Health Service (NHS) Trust, of the UK National Health Service. Procedures involving experiments on human subjects were carried out in accord with the ethical standards of the Institutional Review Board of Imperial College London and in accord with the Helsinki Declaration of 1975. Approval for the study was granted by the NHS Research Ethics Committee London Camberwell St Giles. Consented participants were seen at the West London NHS Trust, where they underwent a range of clinical and cognitive assessments[67]. All ethical regulations relevant to human research participants were followed. The cohort comprised cognitively healthy volunteers aged 40–59 years tested at baseline and 24 months follow-up with the same protocol.

210 individuals (62 male; 148 female) were tested at baseline, with 188 (89.5%) (55 male; 133 female) retained at 2 years follow-up. At baseline, 17 participants were excluded due to lack of participation or contraindications to MRI, 6 due to incidental findings, 24 due to inadequate brain coverage (for details please see the following section on the *functional brain network construction*), 8 due to large head motion (mean framewise displacement >0.4, for details please see the following section), and 2 due to missing *APOE* genotype information. At follow-up, 19 participants were excluded due to decline or contraindications to MRI, 3 due to incidental findings, 5 due to inadequate brain coverage, 10 due to large head motion, and 2 due to missing *APOE* genotype information. Therefore, the dataset for the baseline session was $N = 153$, and the dataset for the follow-up session was $N = 149$ (Figs. 6 and 7c).

Cognitive assessments and risk factors

The Cam-CAN cohort

Cognitive assessment. Cognitive ability was assessed using two measures: fluid intelligence and episodic memory. Fluid intelligence was assessed using the Cattell Culture Fair Test of Fluid Intelligence, which consists of four subtests[68]. To combine this into a single measure, the first principal component across the four subtests was extracted. Episodic memory was assessed using the immediate recall, delayed recall and delayed recognition scores from the Wechsler Logical Memory Task[69]. Similarly, the first principal component of these three scores was used to derive a single memory score for each participant.

The PREVENT cohort

Cognitive assessment. Cognitive function was assessed at baseline and follow-up using the COGNITO neuropsychological battery[70], which is designed to examine information processing across a wide range of cognitive functions in adults of all ages. Additionally, we used the Visual Short-Term Memory Binding Task (VSTMBT), which is sensitive to detecting changes in the pre-symptomatic stages of AD[71]. In total, 13 measures were derived to capture multiple cognitive functions (see SI for details). In previously published work[47,72] we used rotated principal component analysis (rPCA) to cluster these measures into three cognitive components (Supplementary Fig. 4) to boost signal-to-noise ratio and reduce the number of multiple comparisons[73]. Analyses with independent subsets of the PREVENT cohorts showed replicably that episodic and relational memory was the top domain of cognitive variability in this age group[72], and we use this cognitive domain for analyses in this study.

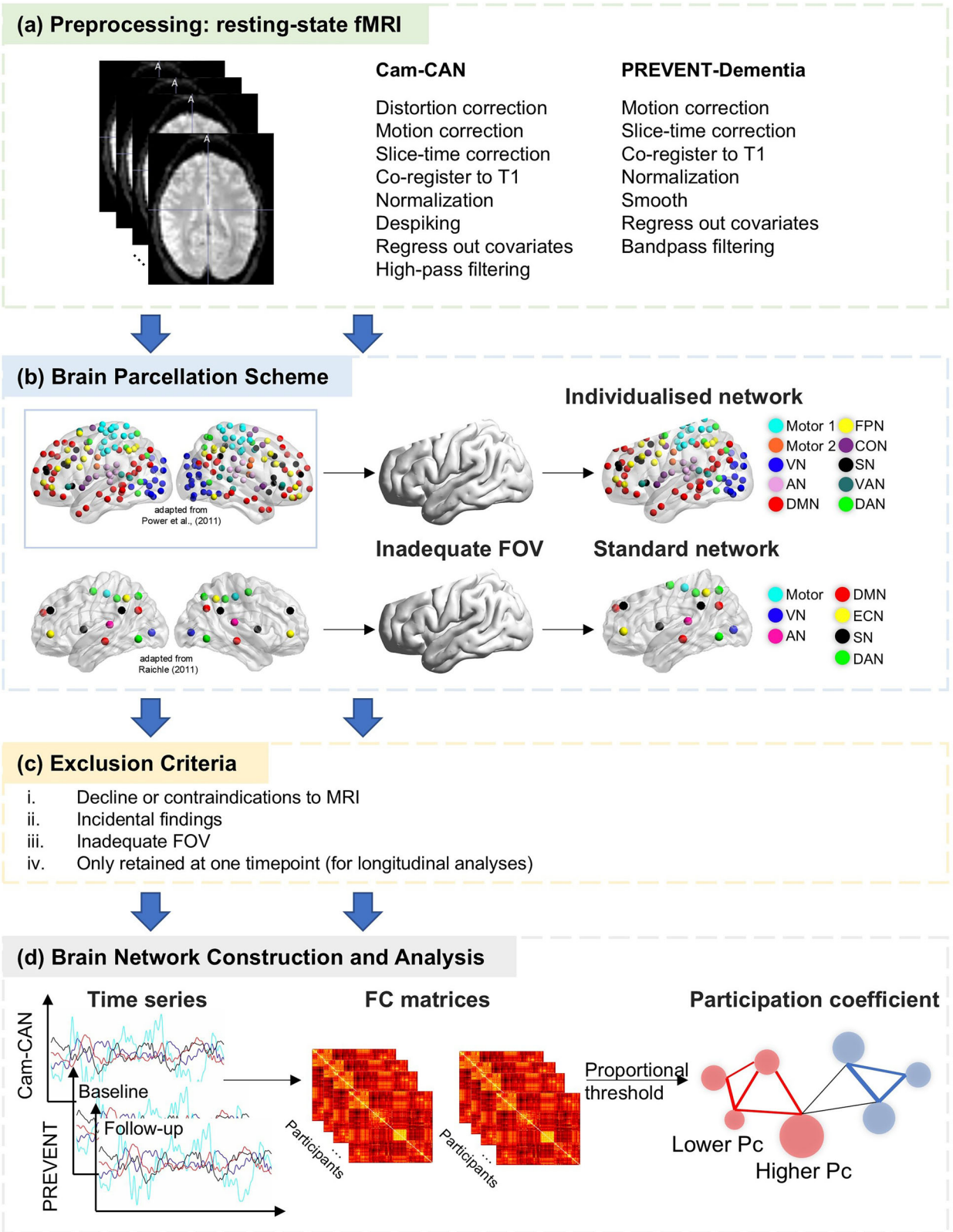

APOE genotyping. The process of *APOE* ε4 allele identification is outlined in detail in Ritchie et al.[8]. In brief, genomic DNA was isolated from blood samples, and *APOE* genotyping was performed. All members of the research and clinical teams were blind to the result of *APOE* genotyping. In this study, *APOE* ε4 risk was determined by ≥1 *APOE* ε4 allele. 54/153 ≥ 1 *APOE* ε4 allele (Table 3). The prevalence of *APOE* ε2ε4 in our cohort is 0.02% (Supplementary Fig. 5). Additional analyses showed that our main findings were not confounded by the inclusion of *APOE* ε2ε4 carriers (see SI).

MRI data acquisition and pre-processing

The Cam-CAN cohort. Imaging data were collected at a single site (MRC-CBU in Cambridge) using a 3 T Siemens TIM Trio scanner with a 32-channel head coil. Full descriptions of the MRI protocols have been

Fig. 7 | Schematic of the study design. a Standard preprocessing steps were performed separately for the Cam-CAN and PREVENT cohorts. **b** Two brain parcellation schemes were adopted to define nodes: the brain atlas of 10 networks (214 brain nodes) by Power et al. (2011) and the coarser brain atlas of 7 networks (33 brain nodes) by Raichle (2011). Results from the Power atlas are reported in the main text for both cohorts. Due to inadequate field of view (FOV) in some participants in the PREVENT cohort, some nodes were dropped and the Raichle atlas was used to corroborate the main results. **c** Several criteria were applied to exclude the inappropriate data for the network analyses. **d** Time courses were extracted based on the predefined brain nodes and correlated to create functional connectivity (FC) matrices using Pearson correlation (r). Proportional thresholds were applied to the FC matrix to generate a sparse matrix for calculating the participation coefficient (Pc) to describe functional segregation. The mock graph illustrates two different networks in red and blue. The node (in red) with lower Pc exhibits strong connections only within its belonging network (edges in red), but no connection to the other network (in blue). By contrast, the node (in purple) with higher Pc exhibits similar connectivity to both networks. Networks whose nodes have low average Pc therefore have higher functional segregation. VN visual, AN auditory, DMN default mode, FPN frontal-parietal control, SN salience, VAN ventral attention, DAN dorsal attention, CON cingulo-opercular control, ECN executive control.

described elsewhere[74]. Resting state fMRI data were acquired using a T2*-weighted echo planar imaging (EPI) sequence with participants resting with their eyes closed. 261 volumes were acquired, and each volume contained 32 axial slices (in descending order) with a slice thickness of 3.7 mm and an interslice gap of 20% [repetition time (TR) = 1970 ms, echo time (TE) = 30 ms, flip angle (FA) = 78°, field of view (FOV) = 192 × 192 mm^2, voxel size = 3 mm × 3 mm × 4.44 mm]. A 3D T1-weighted magnetization prepared rapid gradient-echo image (MPRAGE, TR = 2250 ms, TE = 2.99 ms, FA = 9°, FOV = 256 mm × 240 mm × 192 mm, voxel size = 1 mm^3 isotropic) was also acquired.

Resting-state fMRI data were preprocessed (Fig. 7a) by the Cam-CAN group using a standard preprocessing pipeline with statistical parametric mapping (SPM12, https://www.fil.ion.ucl.ac.uk/spm/software/spm12/) and automatic analysis (AA) software[75]. Details of the pipeline are described in Taylor et al.[74]. Briefly, raw fMRI data were unwarped using field map images for distortion correction due to magnetic field inhomogeneities, realigned for motion correction, and corrected for slice timing. Functional images were then coregistered with T1 structural images and normalised to Montreal Neurological Institute (MNI) standard space via a sample-derived (less age-biased) average using normalisation parameters derived from the Diffeomorphic Anatomical Registration through Exponentiated Lie Algebra (DARTEL) procedure[76]. To further account for the effects of head motion, a wavelet despiking method was applied to remove motion artefacts[77].

For modelling each individual's fMRI timeseries, we applied a general linear model (GLM) including 24 head motion parameters, as well as white matter (WM) and cerebrospinal fluid (CSF) signals, to capture some of the residual effects of head motion and other noise sources. The 24 parameters included six original rigid-body motion parameters, the first-order temporal derivatives of these six parameters, and 12 quadratic terms of the original motion parameters and their derivatives[78]. Finally, high-pass temporal filtering (Gaussian-weighted least-squares straight line fitting, with a cut-off of 100 s) was applied to remove low-frequency artefacts[79].

To further adjust for motion confounds, we calculated frame-wise displacement (FD) motion parameters[80] as the sum of the absolute values of the differences in realignment estimates across successive time points (see SI for full descriptions and the formula), and added the averaged FD across time points as a covariate in the group-level GLMs to capture additional subject-specific motion.

Morphometric brain measures were derived from the T1 images using the Mindboggle pipeline[81]. Grey matter volume (GMV) of 34 brain regions per hemisphere based on the Desikan-Killiany atlas[82] was extracted using the underlying Freesurfer processing pipeline[83]. The mean GMV of these cortical areas was used in this study to represent the structural integrity. Total intracranial volume (TIV) was estimated by SPM12 as the sum of volumes of gray-matter, white-matter and CSF segments.

The PREVENT cohort. Imaging data were obtained as part of a multimodal examinations in a 3 T Siemens Verio MRI scanner and with 32-channel head coil (https://preventdementia.co.uk/for-researchers/). Resting-state fMRI data were acquired with T2*-weighted EPI sequence. 330 volumes were acquired, and each volume contained 35 slices (interleaved acquisition), with slice thickness of 3 mm (TR = 2000 ms, TE = 30 ms, FA = 80°, FOV = 192 × 192 mm^2, voxel size = 3 mm^3 isotropic). A 3D T1-weighted MPRAGE image (160 slices, voxel size = 1 mm^3 isotropic, TR = 2300 ms, TE = 2.98 ms, FOV = 240 × 256 mm^2, FA = 9°) was also acquired. All scans were repeated after approximately 2 years on the same scanner using the same protocol.

Standard preprocessing procedures (Fig. 7a) for resting-state fMRI data were performed with SPM12 and AA software[75] implemented in MATLAB R2019a (The MathWorks, United States). This included slice timing correction, motion correction, co-registration of functional and structural images, normalization into standard MNI space, and spatial smoothing. Spatial normalization was performed using SPM12's segment-and-normalize procedure, whereby the T1 structural was segmented into GM, WM and CSF and normalized to a segmented MNI-152 template. These normalization parameters were then applied to all EPIs. The quality of spatial normalization was visually inspected for each participant and no participants showed a normalization failure. The data were then smoothed with a Gaussian kernel of 6mm full width at half maximum and were temporally band-pass filtered (0.01–0.08 Hz) to remove low-frequency drift and high-frequency physiological noise[84,85]. Finally, to reduce any residual effects of head movement and physiological noise, a GLM was applied with the 24 head movement parameters, as well as WM and CSF signals mentioned above included as covariates[78]. In addition, mean FD was calculated and regressed in the group level analyses[80]. To further control for large head motion at the individual level, we excluded participants with mean FD > 0.4, based on the commonly used cut-off of 0.2–0.5 mm[80,86–89]. This threshold was selected to balance data quality and sample size. The main findings were robust to different cutoffs (see SI).

Morphometric brain measures, including total grey matter volume and intracranial volume, were derived from the T1 images using Freesurfer version 7.1.0[90].

Note that the preprocessing pipelines differed in places between the two cohorts (Fig. 7a), but since we do not directly compare results across cohorts, we do not expect this difference to impact our conclusions. To test this, a harmonized preprocessing pipeline was applied to both cohorts, and the results demonstrate that the main findings are robust and reproducible across different preprocessing strategies (see SI).

Resting-state fMRI data analyses

Functional brain network construction. A graph-theoretic framework was adopted to guide analyses of the functional organisation of brain networks using resting-state fMRI data.

Node definition. 214 brain nodes (spherical, 5 mm diameter) were defined based on a previously published functional system map[43] comprising 10 functional brain networks: SM1 (sensorimotor hand), SM2 (sensorimotor mouth), visual (VIS), auditory (AUD), default mode (DMN), frontal-parietal control (FPN), cingulo-opercular control (CON), ventral attention (VAN), dorsal attention (DAN) and salience network (SN). The timeseries for an ROI was created by averaging the timeseries for every voxel within that ROI.

The resting-state fMRI data from the PREVENT cohort did not have sufficient field of view (FOV) to cover the whole brain in all participants, resulting in the exclusion of some brain nodes in this atlas. To overcome these limitations, we excluded different sets of brain nodes based on

participants' specific FOV and constructed individualised brain networks (Fig. 7b, see also SI for details). To mitigate potential biases arising from differential node coverage, we conducted validation analyses using: the Raichle atlas, which kept the number of nodes the same for all participants; and the normalised Pc, which accounted for the specific modular architecture of each individual's network. This ensured that our findings regarding Pc were robust and not confounded by differences in brain coverage (see SI).

To ensure that participants with poor brain coverage did not bias the network analyses, we excluded participants with less than 80% of the original 214 brain nodes. This threshold was chosen to retain a relatively good number of brain nodes and a satisfactory number of participants to ensure statistical power. The number of retained brain nodes was also included as a covariate in the statistical models to further account for its effect.

Edge definition. Functional connectivity (FC) between pairs of predefined brain nodes was obtained by calculating the Pearson correlation coefficient r of the denoised fMRI time courses derived from these nodes[91], forming the FC matrix (Fig. 7d). The r value was then transformed to z value using Fisher's transformation to improve normality for further statistical analysis. To avoid the formation of artificial anticorrelations, we did not perform a global signal regression[92,93]. Negative connectivity was removed due to its ambiguous meaning[93,94]. The main results remained consistent when we defined edges using mutual information[95], which captures both linear and nonlinear dependencies and is less sensitive to the presence or absence of global signal regression (see SI).

Thresholding the FC matrix to form a sparse matrix is important to remove spurious connections[96]. FC matrices were therefore thresholded from 5% to 50% connection density with a 5% interval, as graphs become more random above a threshold of 50%[97]. The area under the curve (AUC) for the graph theoretical measure across all thresholds was calculated to provide a scalar that does not depend on a specific threshold selection[98,99].

Participation coefficient

A localised measure called the "participation coefficient" (Pc)[10,100] was used to measure network segregation. The use of the participation coefficient is grounded in its established interpretation as a network-level index of functional segregation when averaged within predefined modules. We explicitly defined segregation as the extent to which nodes within a network preferentially connect to each other rather than to nodes in other networks. Under this definition, increased Pc at the network or global level reflects reduced segregation, whereas lower Pc reflects stronger network segregation. The Pc of a brain node represents the distribution of its connections across separate networks[101,102], defined as:

$$P_i = 1 - \sum_{m \in M} \left(\frac{k_i^w(m)}{k_i^w} \right)^2,$$

where m is a network in a set of networks M, $k_i^w(m)$ are the weighted connections of node i with all nodes in network m and k_i^w is the total weighted connections involving node i. A value of P_i close to 0 indicates that most of node i's connections are restricted to its own network, whereas a value close to 1 indicates that node i's connections are more equally distributed among different networks (Fig. 7d). To quantify the segregation of individual networks, we averaged P_i across brain nodes that were assigned to the same network. The average P_i of nodes across the whole brain was used to quantify global network segregation[10,100].

Additional metrics

Two other global metrics—global efficiency[103] and modularity[104]—were also investigated to test whether the global network topology remains largely intact in at-risk individuals at midlife (see SI). Additionally, raw connectivity strength—global mean functional connectivity (mean FC)—was assessed in relation to risk in order to isolate any potential effects of risk on Pc values (see SI).

Statistics and reproducibility

The Cam-CAN cohort. All statistical analyses were performed using the R software. All regressors in the linear models were Z-scored. First, we examined the relationship between global network segregation and a second-order polynomial expansion of age using multiple regression, with sex and mean FD as covariates of no interest (the latter to further control for any residual effects of head motion in fMRI data). We also performed second regression where we additionally controlled for GMV and TIV, to test whether the segregation relates to age even beyond age-related differences in GM atrophy. This approach controls for age-related brain atrophy by accounting for individual brain size. Then we examined the relationship between segregation and (1) fluid intelligence and (2) episodic memory (see above). Initial models controlled for sex and FD, followed by additional models incorporating age (including its second-order effects) as a covariate. This approach allowed us to test whether segregation relates to cognitive performance above and beyond age. Finally, we investigated the linear and/or quadratic effect of age on functional segregation of each network separately, with sex and mean FD as covariates, in order to select networks that might be most sensitive to AD risk in the PREVENT cohort. Multiple comparisons across the 10 individual networks were Bonferroni-corrected.

The PREVENT cohort. The normality of the data was assessed by combining the visualization of a quantile–quantile plot and the Shapiro–Wilk test. Demographic and clinical information of this study cohort was analysed across risk groups, using χ^2 tests for categorical variables and Mann–Whitney U tests for continuous variables, given that they were not normally distributed.

Cross-sectional effects. Baseline data were used to examine cross-sectional effects. We first examined the effect of *APOE* ε4 genotype using multiple regression, adjusting for age, sex, mean FD, as confounds, as well as the number of brain nodes (which differed across participants for reasons given above, and might affect segregation estimates). This was done on global Pc, as well as the individual networks identified as showing effects of age in the Cam-CAN cohort. Multiple comparisons were Bonferroni-corrected for the number of networks tested. For the global Pc, we also conducted another regression model with GMV and TIV added as additional covariates. Then, any networks that showed a significant effect of *APOE* ε4 was further assessed in relation to cognitive performance, using the three cognitive factors extracted from the COGNITO battery (see above). Multiple comparisons were again Bonferroni-corrected for the number of networks tested.

Longitudinal effects. Those networks that showed cross-sectional segregation differences related to *APOE* ε4 genotype at baseline were further assessed for longitudinal change over 2 years using a mixed effects model. Specifically, time (a binary variable indicating baseline or follow-up), *APOE* ε4 genotype and their interaction were included as predictors. Covariates included mean FD and number of brain nodes at each time point, age at baseline, sex, and participant as a random intercept. When a significant time × risk interaction was identified, paired t-tests were performed to determine which risk groups showed significant changes in network Pc between baseline and follow-up. In addition, we examined whether longitudinal changes in network segregation were related to longitudinal changes in cognitive performance. In this mixed effect model, cognition at both time points was the dependent variable, while network Pc at both time points, the risk factor, and their interaction were predictors, as well as the same covariates as above.

Validation analyses for both the Cam-CAN and the PREVENT cohorts

We used an alternative parcellation scheme (Fig. 7b) that included a smaller number of key brain nodes (node = 33, spherical, 5 mm diameter) in 7

predefined brain networks[105] to validate our main findings. Specifically, for the PREVENT cohort, by using this parcellation scheme, we were able to retain all brain nodes and exclude participants without full coverage of these nodes, leading to a different subset of participants compared to the main analyses (based on the 80% node retention threshold in the Power atlas).

Reporting summary

Further information on research design is available in the Nature Portfolio Reporting Summary linked to this article.

Data availability

Data are available to access through a data request on the study website (www.preventdementia.co.uk); the ADDI platform (https://doi.org/10.34688/PREVENTMAIN_BASELINE_700V1); Dementia Platforms UK; and the Global Alzheimer's Association Network. Numerical source data underlying graphs in the manuscript can be found in supplementary data.

Code availability

The custom code reproducing all statistical tests, graphs, and tables reported in the manuscript is publicly available in https://github.com/fengdeng315/Segregation_risk_age. For code to reproduce neuroimaging preprocessing and network construction, please contact Dr. Lorina Naci (nacil@tcd.ie).

Received: 11 June 2025; Accepted: 6 May 2026;
Published online: 19 May 2026

References

1. World Health Organization. *Global status report on the public health response to dementia*. Geneva: World Health Organization (2021). Available at: https://www.who.int/publications/i/item/9789240033245.
2. Jansen, W. J. et al. Prevalence of cerebral amyloid pathology in persons without dementia: a meta-analysis. *JAMA* **313**, 1924–1938 (2015).
3. Sperling, R. A. et al. Toward defining the preclinical stages of Alzheimer's disease: recommendations from the National Institute on Aging-Alzheimer's Association workgroups on diagnostic guidelines for Alzheimer's disease. *Alzheimers Dement* **7**, 280–292 (2011).
4. Barnes, D. E. & Yaffe, K. The projected effect of risk factor reduction on Alzheimer's disease prevalence. *Lancet Neurol.* **10**, 819–828 (2011).
5. Livingston, G. et al. Dementia prevention, intervention, and care. *Lancet* **390**, 2673–2734 (2017).
6. Ritchie, K. et al. Designing prevention programmes to reduce incidence of dementia: prospective cohort study of modifiable risk factors. *BMJ* **341**, c3885 (2010).
7. Irwin, K., Sexton, C., Daniel, T., Lawlor, B. & Naci, L. Healthy aging and dementia: two roads diverging in midlife? *Front Aging Neurosci.* **10**, 275 (2018).
8. Ritchie, K. et al. The midlife cognitive profiles of adults at high risk of late-onset Alzheimer's disease: the PREVENT study. *Alzheimers Dement* **13**, 1089–1097 (2017).
9. Geerligs, L., Maurits, N. M., Renken, R. J. & Lorist, M. M. Reduced specificity of functional connectivity in the aging brain during task performance. *Hum. Brain Mapp.* **35**, 319–330 (2014).
10. Chan, M. Y., Park, D. C., Savalia, N. K., Petersen, S. E. & Wig, G. S. Decreased segregation of brain systems across the healthy adult lifespan. *Proc. Natl. Acad. Sci. USA* **111**, E4997–E5006 (2014).
11. Wig, G. S. Segregated systems of human brain networks. *Trends Cogn. Sci.* **21**, 981–996 (2017).
12. Raykov, P. P., Knights, E. & Henson, R. N. Does functional system segregation mediate the effects of lifestyle on cognition in older adults? *Neurobiol. Aging* **134**, 126–134 (2024).
13. Chong, J. S. X. et al. Longitudinal changes in the cerebral cortex functional organization of healthy elderly. *J. Neurosci.* **39**, 5534–5550 (2019).
14. King, B. R. et al. Age-related declines in motor performance are associated with decreased segregation of large-scale resting state brain networks. *Cereb. Cortex* **28**, 4390–4402 (2018).
15. Kong, T. S. et al. Age-related differences in functional brain network segregation are consistent with a cascade of cerebrovascular, structural, and cognitive effects. *Netw. Neurosci.* **4**, 89–114 (2020).
16. Manza, P. et al. Brain network segregation and glucose energy utilization: relevance for age-related differences in cognitive function. *Cereb. Cortex* **30**, 5930–5942 (2020).
17. Pedersen, R. et al. When functional blurring becomes deleterious: reduced system segregation is associated with less white matter integrity and cognitive decline in aging. *Neuroimage* **242**, 118449 (2021).
18. Varangis, E., Habeck, C. G., Razlighi, Q. R. & Stern, Y. The effect of aging on resting state connectivity of predefined networks in the brain. *Front Aging Neurosci.* **11**, 234 (2019).
19. Cassady, K. et al. Sensorimotor network segregation declines with age and is linked to GABA and to sensorimotor performance. *Neuroimage* **186**, 234–244 (2019).
20. Cassady, K. et al. Network segregation varies with neural distinctiveness in sensorimotor cortex. *Neuroimage* **212**, 116663 (2020).
21. Chan, M. Y. et al. Long-term prognosis and educational determinants of brain network decline in older adult individuals. *Nat. Aging* **1**, 1053–1067 (2021).
22. Gallen, C. L. et al. Modular brain network organization predicts response to cognitive training in older adults. *PLoS ONE* **11**, e0169015 (2016).
23. Arnemann, K. L. et al. Functional brain network modularity predicts response to cognitive training after brain injury. *Neurology* **84**, 1568–1574 (2015).
24. Stern, Y. Cognitive reserve in ageing and Alzheimer's disease. *Lancet Neurol.* **11**, 1006–1012 (2012).
25. Brier, M. R. et al. Functional connectivity and graph theory in preclinical Alzheimer's disease. *Neurobiol. Aging* **35**, 757–768 (2014).
26. Ewers, M. et al. Segregation of functional networks is associated with cognitive resilience in Alzheimer's disease. *Brain* **144**, 2176–2185 (2021).
27. Ng, K. K. et al. Functional segregation loss over time is moderated by APOE genotype in healthy elderly. *Hum. Brain Mapp.* **39**, 2742–2752 (2018).
28. Lambert, J. C. et al. Meta-analysis of 74,046 individuals identifies 11 new susceptibility loci for Alzheimer's disease. *Nat. Genet.* **45**, 1452–1458 (2013).
29. Farràs-Permanyer, L. et al. Estimation of brain functional connectivity in patients with mild cognitive impairment. *Brain Sci.* **9**, 350 (2019).
30. Jiao, Z., Gao, P., Ji, Y. & Shi, H. Integration and segregation of dynamic functional connectivity states for mild cognitive impairment revealed by graph theory indicators. *Contrast Media Mol. Imaging* **2021**, 6890024 (2021).
31. Dai, Z. et al. Disrupted structural and functional brain networks in Alzheimer's disease. *Neurobiol. Aging* **75**, 71–82 (2019).
32. Foo, H. et al. Genetic influence on ageing-related changes in resting-state brain functional networks in healthy adults: a systematic review. *Neurosci. Biobehav Rev.* **113**, 98–110 (2020).
33. Betzel, R. F. et al. Changes in structural and functional connectivity among resting-state networks across the human lifespan. *Neuroimage* **102**, 345–357 (2014).
34. Geerligs, L., Renken, R. J., Saliasi, E., Maurits, N. M. & Lorist, M. M. A brain-wide study of age-related changes in functional connectivity. *Cereb. Cortex* **25**, 1987–1999 (2015).
35. Siman-Tov, T. et al. Early age-related functional connectivity decline in high-order cognitive networks. *Front Aging Neurosci.* **8**, 330 (2016).

36. Greicius, M. D., Srivastava, G., Reiss, A. L. & Menon, V. Default-mode network activity distinguishes Alzheimer's disease from healthy aging: evidence from functional MRI. *Proc. Natl. Acad. Sci. USA* **101**, 4637–4642 (2004).
37. Kucikova, L. et al. Resting-state brain connectivity in healthy young and middle-aged adults at risk of progressive Alzheimer's disease. *Neurosci. Biobehav Rev.* **129**, 142–153 (2021).
38. Márquez, F. & Yassa, M. A. Neuroimaging biomarkers for Alzheimer's disease. *Mol. Neurodegener.* **14**, 21 (2019).
39. Rombouts, S. A. R. B., Barkhof, F., Goekoop, R., Stam, C. J. & Scheltens, P. Altered resting state networks in mild cognitive impairment and mild Alzheimer's disease: an fMRI study. *Hum. Brain Mapp.* **26**, 231–239 (2005).
40. Buckner, R. L. et al. Molecular, structural, and functional characterization of Alzheimer's disease: evidence for a relationship between default activity, amyloid, and memory. *J. Neurosci.* **25**, 7709–7717 (2005).
41. Dickerson, B. C. et al. The cortical signature of Alzheimer's disease: regionally specific cortical thinning relates to symptom severity in very mild to mild AD dementia and is detectable in asymptomatic amyloid-positive individuals. *Cereb. Cortex* **19**, 497–510 (2009).
42. Minoshima, S. et al. Metabolic reduction in the posterior cingulate cortex in very early Alzheimer's disease. *Ann. Neurol.* **42**, 85–94 (1997).
43. Power, J. D. et al. Functional network organization of the human brain. *Neuron* **72**, 665–678 (2011).
44. Habib, M. et al. Functional neuroimaging findings in healthy middle-aged adults at risk of Alzheimer's disease. *Ageing Res. Rev.* **36**, 88–104 (2017).
45. Koch, W. et al. Diagnostic power of default mode network resting state fMRI in the detection of Alzheimer's disease. *Neurobiol. Aging* **33**, 466–478 (2012).
46. Sorg, C. et al. Selective changes of resting-state networks in individuals at risk for Alzheimer's disease. *Proc. Natl. Acad. Sci. USA* **104**, 18760–18765 (2007).
47. Deng, F. et al. Cardiovascular risk of dementia is associated with brain–behaviour changes in cognitively healthy, middle-aged individuals. *Neurobiol. Aging* **144**, 78–92 (2024).
48. Gharbi-Meliani, A. et al. The association of APOE ε4 with cognitive function over the adult life course and incidence of dementia: 20 years follow-up of the Whitehall II study. *Alzheimers Res. Ther.* **13**, 5 (2021).
49. Zokaei, N. et al. Short-term memory advantage for brief durations in human APOE ε4 carriers. *Sci. Rep.* **10**, 9503 (2020).
50. Dounavi, M.-E. et al. Evidence of cerebral hemodynamic dysregulation in middle-aged APOE ε4 carriers: the PREVENT-Dementia study. *J. Cereb. Blood Flow. Metab.* **41**, 2844–2855 (2021).
51. Mak, E. et al. Proximity to dementia onset and multi-modal neuroimaging changes: the prevent-dementia study. *NeuroImage* **229**, 117749 (2021).
52. McKiernan, E. F. et al. Regional hyperperfusion in cognitively normal APOE ε4 allele carriers in mid-life: analysis of ASL pilot data from the PREVENT-Dementia cohort. *J. Neurol. Neurosurg. Psychiatry* **91**, 861–866 (2020).
53. Cacciaglia, R. et al. Genotypic effects of APOE-ε4 on resting-state connectivity in cognitively intact individuals support functional brain compensation. *Cereb. Cortex* **33**, 2748–2760 (2023).
54. Westlye, E. T., Lundervold, A., Rootwelt, H., Lundervold, A. J. & Westlye, L. T. Increased hippocampal default mode synchronization during rest in middle-aged and elderly APOE ε4 carriers: relationships with memory performance. *J. Neurosci.* **31**, 7775–7783 (2011).
55. Koelewijn, L. et al. Oscillatory hyperactivity and hyperconnectivity in young APOE-ε4 carriers and hypoconnectivity in Alzheimer's disease. *Elife* **8**, e36011 (2019).
56. Koelewijn, L. et al. Alzheimer's disease disrupts alpha and beta-band resting-state oscillatory network connectivity. *Clin. Neurophysiol.* **128**, 2347–2357 (2017).
57. Williams, G. C. Pleiotropy, natural selection, and the evolution of senescence. *Evolution* **11**, 398–411 (1957).
58. Kantarovich, K. et al. White matter lesion load is associated with lower within- and greater between-network connectivity across older age. *Neurobiol. Aging* **112**, 170–180 (2022).
59. Pedersen, R. et al. Dopamine D1-receptor organization contributes to functional brain architecture. *J. Neurosci.* **44**, e0621232024 (2024).
60. Dickerson, B. C. & Sperling, R. A. Large-scale functional brain network abnormalities in Alzheimer's disease: insights from functional neuroimaging. *Behav. Neurol.* **21**, 63–75 (2009).
61. Jack, C. R. et al. Tracking pathophysiological processes in Alzheimer's disease: an updated hypothetical model of dynamic biomarkers. *Lancet Neurol.* **12**, 207–216 (2013).
62. Shaw, L. M. et al. Cerebrospinal fluid biomarker signature in Alzheimer's disease neuroimaging initiative subjects. *Ann. Neurol.* **65**, 403–413 (2009).
63. Palmqvist, S. et al. Performance of fully automated plasma assays as screening tests for Alzheimer disease-related β-amyloid status. *JAMA Neurol.* **76**, 1060–1069 (2019).
64. Palmqvist, S. et al. Discriminative accuracy of plasma phospho-tau217 for Alzheimer disease vs other neurodegenerative disorders. *JAMA* **324**, 772–781 (2020).
65. Shafto, M. A. et al. The Cambridge Centre for Ageing and Neuroscience (Cam-CAN) study protocol: a cross-sectional, lifespan, multidisciplinary examination of healthy cognitive ageing. *BMC Neurol.* **14**, 204 (2014).
66. Ritchie, C. W. et al. The PREVENT dementia programme: baseline demographic, lifestyle, imaging and cognitive data from a midlife cohort study investigating risk factors for dementia. *Brain Commun.* **6**, fcae189 (2024).
67. Ritchie, C. W. & Ritchie, K. The PREVENT study: a prospective cohort study to identify mid-life biomarkers of late-onset Alzheimer's disease. *BMJ Open* **2**, e001893 (2012).
68. Cattell, R. B. *Abilities: Their Structure, Growth, and Action*. xxii, 583 (Houghton Mifflin, 1971).
69. Wechsler, D. A standardized memory scale for clinical use. *J. Psychol.: Interdiscip. Appl.* **19**, 87–95 (1945).
70. Ritchie, K. et al. COGNITO: computerized assessment of information processing. *J. Psychol. Psychother.* **4**, 136 (2014).
71. Parra, M. A. et al. Visual short-term memory binding deficits in familial Alzheimer's disease. *Brain* **133**, 2702–2713 (2010).
72. Qi, Q. et al. Associations between sex and lifestyle activities with cognitive reserve in mid-life adults with genetic risk for Alzheimer's disease. *Alzheimer's. Res. Ther.* **16**, 246 (2024).
73. Jolliffe, I. T. & Cadima, J. Principal component analysis: a review and recent developments. *Philos. Trans. A Math. Phys. Eng. Sci.* **374**, 20150202 (2016).
74. Taylor, J. R. et al. The Cambridge Centre for Ageing and Neuroscience (Cam-CAN) data repository: structural and functional MRI, MEG, and cognitive data from a cross-sectional adult lifespan sample. *Neuroimage* **144**, 262–269 (2017).
75. Cusack, R. et al. Automatic analysis (aa): efficient neuroimaging workflows and parallel processing using Matlab and XML. *Front Neuroinform* **8**, 90 (2014).
76. Ashburner, J. A fast diffeomorphic image registration algorithm. *Neuroimage* **38**, 95–113 (2007).
77. Patel, A. X. et al. A wavelet method for modeling and despiking motion artifacts from resting-state fMRI time series. *NeuroImage* **95**, 287–304 (2014).
78. Satterthwaite, T. D. et al. An improved framework for confound regression and filtering for control of motion artifact in the

preprocessing of resting-state functional connectivity data. *Neuroimage* **64**, 240–256 (2013).
79. Geerligs, L. & Tsvetanov, K. A. Cam-Can, null & Henson, R. N. Challenges in measuring individual differences in functional connectivity using fMRI: the case of healthy aging. *Hum. Brain Mapp.* **38**, 4125–4156 (2017).
80. Power, J. D., Barnes, K. A., Snyder, A. Z., Schlaggar, B. L. & Petersen, S. E. Spurious but systematic correlations in functional connectivity MRI networks arise from subject motion. *Neuroimage* **59**, 2142–2154 (2012).
81. Klein, A. et al. Mindboggling morphometry of human brains. *PLoS Comput. Biol.* **13**, e1005350 (2017).
82. Desikan, R. S. et al. An automated labeling system for subdividing the human cerebral cortex on MRI scans into gyral based regions of interest. *Neuroimage* **31**, 968–980 (2006).
83. Klein, A. & Tourville, J. 101 labeled brain images and a consistent human cortical labeling protocol. *Front Neurosci.* **6**, 171 (2012).
84. Salvador, R. et al. A simple view of the brain through a frequency-specific functional connectivity measure. *Neuroimage* **39**, 279–289 (2008).
85. Zuo, X.-N. et al. The oscillating brain: complex and reliable. *Neuroimage* **49**, 1432–1445 (2010).
86. Kim, J.-H., De Asis-Cruz, J., Kapse, K. & Limperopoulos, C. Systematic evaluation of head motion on resting-state functional connectivity MRI in the neonate. *Hum. Brain Mapp.* **44**, 1934–1948 (2023).
87. Power, J. D. et al. Methods to detect, characterize, and remove motion artifact in resting state fMRI. *Neuroimage* **84**, 320–341 (2014).
88. Siegel, J. S. et al. Statistical improvements in functional magnetic resonance imaging analyses produced by censoring high-motion data points. *Hum. Brain Mapp.* **35**, 1981–1996 (2014).
89. Yan, C.-G. et al. A comprehensive assessment of regional variation in the impact of head micromovements on functional connectomics. *Neuroimage* **76**, 183–201 (2013).
90. Dounavi, M.-E. et al. Macrostructural brain alterations at midlife are connected to cardiovascular and not inherited risk of future dementia: the PREVENT-Dementia study. *J. Neurol.* **269**, 4299–4309 (2022).
91. van den Heuvel, M. P. & Hulshoff Pol, H. E. Exploring the brain network: a review on resting-state fMRI functional connectivity. *Eur. Neuropsychopharmacol.* **20**, 519–534 (2010).
92. Anderson, J. S. et al. Network anticorrelations, global regression, and phase-shifted soft tissue correction. *Hum. Brain Mapp.* **32**, 919–934 (2011).
93. Murphy, K., Birn, R. M., Handwerker, D. A., Jones, T. B. & Bandettini, P. A. The impact of global signal regression on resting state correlations: are anti-correlated networks introduced? *Neuroimage* **44**, 893–905 (2009).
94. Chai, X. J., Castañón, A. N., Ongür, D. & Whitfield-Gabrieli, S. Anticorrelations in resting state networks without global signal regression. *Neuroimage* **59**, 1420–1428 (2012).
95. Ince, R. A. A. et al. A statistical framework for neuroimaging data analysis based on mutual information estimated via a Gaussian copula. *Hum. Brain Mapp.* **38**, 1541–1573 (2017).
96. van den Heuvel, M. P. et al. Proportional thresholding in resting-state fMRI functional connectivity networks and consequences for patient-control connectome studies: issues and recommendations. *Neuroimage* **152**, 437–449 (2017).
97. Humphries, M. D., Gurney, K. & Prescott, T. J. The brainstem reticular formation is a small-world, not scale-free, network. *Proc. Biol. Sci.* **273**, 503–511 (2006).
98. Achard, S. & Bullmore, E. Efficiency and cost of economical brain functional networks. *PLoS Comput. Biol.* **3**, e17 (2007).
99. Wang, J. et al. Parcellation-dependent small-world brain functional networks: a resting-state fMRI study. *Hum. Brain Mapp.* **30**, 1511–1523 (2009).
100. Rubinov, M. & Sporns, O. Complex network measures of brain connectivity: uses and interpretations. *Neuroimage* **52**, 1059–1069 (2010).
101. Guimerà, R. & Nunes Amaral, L. A. Functional cartography of complex metabolic networks. *Nature* **433**, 895–900 (2005).
102. Power, J. D., Schlaggar, B. L., Lessov-Schlaggar, C. N. & Petersen, S. E. Evidence for hubs in human functional brain networks. *Neuron* **79**, 798–813 (2013).
103. Latora, V. & Marchiori, M. Efficient behavior of small-world networks. *Phys. Rev. Lett.* **87**, 198701 (2001).
104. Newman, M. E. J. Modularity and community structure in networks. *Proc. Natl. Acad. Sci. USA* **103**, 8577–8582 (2006).
105. Raichle, M. E. The restless brain. *Brain Connect* **1**, 3–12 (2011).

Acknowledgements

We thank all PREVENT-Dementia participants for their enthusiastic participation in this study. We also thank the Research Delivery service at West London NHS Trust and the Wolfson Clinical Imaging Facility at Imperial College London for their support in running the study.

Author contributions

F.D. contributed writing—original draft, review & editing, visualization, investigation, formal analysis, data curation and conceptualization. R.N.H. contributed writing—review & editing and methodology. G.M. contributed writing—review & editing and methodology. P.M. contributed writing—review & editing, project administration. J.T.O. contributed writing—review & editing, project administration and funding acquisition. C.W.R. contributed writing—review & editing, project administration and funding acquisition. B.L. contributed writing—review & editing, project administration and funding acquisition. L.N. contributed writing—original draft, review & editing, supervision, project administration, methodology, investigation, funding acquisition and conceptualization.

Funding

F.D. discloses support for the research of this work from the National Natural Science Foundation of China (grant number 32400902) and the Provost PhD Award Scheme from Trinity College Dublin, to L.N. L.N. discloses support for the research of this work from the Health Research Board Individual Led Project Grant (ILP-POR-2024-057), and the Research Ireland Frontiers for the Future Grant (23/FFP-A/11888). R.N.H. discloses support for publication of this work from the UK Medical Research Council [SUAG/046/G101400]. J.O.B. discloses support for the research of this work from the NIHR Cambridge Biomedical Research Centre. The PREVENT-Dementia study is supported by the UK Alzheimer's Society (grant numbers 178 and 264), the US Alzheimer's Association (grant number TriBEKa-17-519007) and philanthropic donations. The PREVENT Dementia study at Trinity College Dublin was in part supported by a project grant from GBHI and philanthropic donations from Trinity Foundation. Cam-CAN was initially supported by the Biotechnology and Biological Sciences Research Council Grant BB/H008217/1, then received further contributions from the European Union's Horizon 2020 research and innovation programme ('LifeBrain', Grant Agreement No. 732592) and intramural funding to the MRC Cognition & Brain Sciences Unit [SUAG/046/G101400]. For the purpose of open access, the author has applied a Creative Commons Attribution (CC BY) licence to any Author Accepted Manuscript version arising from this submission.

Competing interests

The authors declare no competing interests.

Additional information

Supplementary information The online version contains supplementary material available at https://doi.org/10.1038/s42003-026-10282-0.

Correspondence and requests for materials should be addressed to Lorina Naci.

Peer review information *Communications Biology* thanks Caishui Yang, Roser Sala-Llonch and the other, anonymous, reviewer(s) for their contribution to the peer review of this work. Primary Handling Editor: Joao Valente.